JACS
JOURNAL OF THE AMERICAN CHEMICAL SOCIETY
Communication
pubs.acs.org/JACS

# Chemical Vapor Deposition of Large-Size Monolayer $MoSe_2$ Crystals on Molten Glass

Jianyi Chen,[†] Xiaoxu Zhao,[†] Sherman J. R. Tan,[†] Hai Xu,[†] Bo Wu,[†] Bo Liu,[†,‡] Deyi Fu,[†] Wei Fu,[†] Dechao Geng,[†] Yanpeng Liu,[†] Wei Liu,[†] Wei Tang,[†] Linjun Li,[†] Wu Zhou,[§,⊥] Tze Chien Sum,[‡] and Kian Ping Loh*[,†]

[†]Graphene Research Centre and Department of Chemistry, National University of Singapore, 6 Science Drive 2, 117546 Singapore
[‡]Division of Physics and Applied Physics, School of Physical and Mathematical Sciences, Nanyang Technological University, 21 Nanyang Link, 637371 Singapore
[§]School of Physical Sciences, CAS Key Laboratory of Vacuum Sciences, University of Chinese Academy of Sciences, Beijing 100049, China
[⊥]Materials Science and Technology Division, Oak Ridge National Laboratory, Oak Ridge, Tennessee 37831, United States

Supporting Information

**ABSTRACT:** We report the fast growth of high-quality millimeter-size monolayer $MoSe_2$ crystals on molten glass using an ambient pressure CVD system. We found that the isotropic surface of molten glass suppresses nucleation events and greatly improves the growth of large crystalline domains. Triangular monolayer $MoSe_2$ crystals with sizes reaching ~2.5 mm, and with a room-temperature carrier mobility up to ~95 $cm^2/(V·s)$, can be synthesized in 5 min. The method can also be used to synthesize millimeter-size monolayer $MoS_2$ crystals. Our results demonstrate that "liquid-state" glass is a highly promising substrate for the low-cost growth of high-quality large-size 2D transition metal dichalcogenides (TMDs).

Two-dimensional (2D) transition metal dichalcogenides (TMDs) have attracted much attention due to their excellent electronic and optical properties.[1] The large spin−orbit coupling allows spin-valley coupling to be observed in TMDs.[2] At monolayer thickness, the band structures of some TMDs transit from indirect to direct band gap.[1] These properties render TMDs attractive for applications in optoelectronics, valleytronic and spintronic devices.[3] To obtain high-quality TMD monolayers, many approaches have been applied, including mechanical exfoliation, chemical exfoliation and chemical vapor deposition.[1] Among them, the CVD approach has the greatest potential for scaled-up production. However, due to the lack of low-cost chemically inert metal substrates, almost all the CVD methods reported to date used solid dielectric substrates. It is widely postulated that the nucleation of crystallites occurs preferentially at impurities or defect sites on solid substrates, such that mosaic polycrystalline films inevitably form on with a high density of defects. To promote large-sized single crystal domain, complicated growth techniques or surface treatment methods have to be employed to suppress nucleation events.[4] On the other hand, the growth of graphene on molten metallic substrates allows hexagonal crystallites to be assembled in highly aligned manner.[5] Recently, the growth of polycrystalline graphene film on glass has been attempted using the molten glass-substrate approach;[6] however, there has been no reports of large area TMD crystal growth on glass. The growth of 2D materials on molten glass has not received the attention it deserves to date, despite the advantage of glass as a low cost, transparent substrate for photonic applications.

Here, we report the successful growth of millimeter-size high-quality monolayer $MoSe_2$ crystals on molten glass. The melting and regeneration of glass generate a smooth surface, with a signficantly reduced defect density, and thus enable low density nucleation for large crystal domain growth. Triangle-shaped monolayer $MoSe_2$ domains with widths reaching several millimeters can be grown in 5 min. The method can also be used to synthesize millimeter-size monolayer $MoS_2$ crystals, suggesting the generic applicability of this method.

As described in Figure 1a and Figure S1, glass substrates were placed in a quartz tube mounted inside a tube furnace for $MoSe_2$ synthesis. The present setup uses a piece of $SiO_2/Si$ with a piece of Mo foils on the surface to hold molten glass, which are put face-up above the $MoO_3$ source. Prior to the growth process, solid glass plates were cleaned in deionized water, acetone, isopropyl alcohol, followed by 5 min of $O_2$ plasma to remove the impurities absorbed on the surface. During the ramp up period, solid glass melts and a clean atomically flat liquid surface is obtained. The melting process erases the high-energy sites such as defects, kinks, and asperites,[6] thus facilitating the growth of large-size high-quality $MoSe_2$ crystals. 20-sccm Ar is used as the carrier gas, and a small amount of $H_2$, a reducing agent for $MoO_3$, is used to control the start and end point of the reaction. The CVD growth process is carried out at ambient pressure, and the temperatures of selenium powders and molten glass during growth are kept at 280 and 1050 °C, respectively.

Figure 1b presents a photograph of $MoSe_2$ crystals grown on molten glass. A millimeter-scale triangular $MoSe_2$ crystal marked by green frame can be seen by eye. Figure 1c shows the typical optical microscopy (OM) image of $MoSe_2$ crystals.

**Received:** November 24, 2016
**Published:** January 4, 2017

ACS Publications © 2017 American Chemical Society



DOI: 10.1021/jacs.6b12156
J. Am. Chem. Soc. 2017, 139, 1073−1076

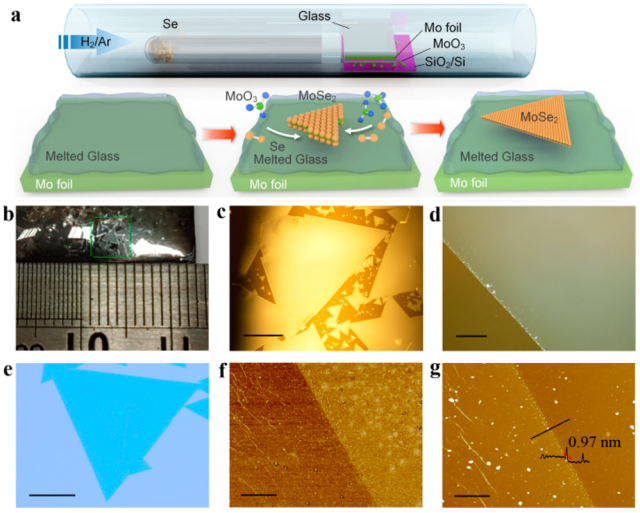


**Figure 1.** Synthesis process and morphology of $MoSe_2$ monolayers. (a) Scheme showing CVD process for the synthesis of $MoSe_2$ crystals on molten glass. (b) Photograph of $MoSe_2$ crystals grown on molten glass. (c,d) Optical images of $MoSe_2$ crystals grown on molten glass. Scale bar 500 $\mu$m in panel c and 10 $\mu$m in panel d. (e) Optical image of $MoSe_2$ crystals transferred onto $SiO_2$/Si substrates. Scale bar 500 $\mu$m. (f,g) AFM phase (f) and height (g) images of $MoSe_2$ crystals. Scale bar 1 $\mu$m.

The straight edges suggest that these triangular $MoSe_2$ crystals have a uniform molybdenum zigzag (Mo-zz) edge structure.[7] The growth of $MoSe_2$ crystals can occur in a wide temperature range from 700 to 1050 °C (Figure S2). With increasing growth temperature, the $MoSe_2$ nucleation density decreases and the grain size increases. At 1050 °C, the nucleation density can be controlled below 20 nuclei $cm^{-2}$. The ratio of Ar/$H_2$ gas mixture influences the shape and quality of $MoSe_2$ crystals: increasing the concentration of $H_2$ (>30%) enhances the etching of $MoSe_2$ crystals, whereas reducing it (<9%) promotes the formation of hexagonally shaped $MoSe_2$ crystals (Figure S3). However, after 5 min growth at a suitable $H_2$ flow (~13%), the dielectric surface is covered mainly by large-size $MoSe_2$ monolayers (from several hundred micrometers to several millimeters) (Figure S4). Further growth (>15 min) enlarges the number of $MoSe_2$ sheets, and many nearest-neighbor $MoSe_2$ sheets link together, resulting in a continuous film. Unlike graphene and GaSe grown on liquid metals,[5,8] the as-synthesized $MoSe_2$ domains are not self-aligned into an ordered structure, due probably to its high-speed growth. Figure 1d shows a high-magnification OM of the CVD-grown $MoSe_2$ crystals. The uniform color contrast indicates the large-size crystals are of uniform thickness. The as-grown $MoSe_2$ crystals can be transferred from molten glass onto other substrates by using PMMA techniques (Figure 1e, Figure S5). When imaged using atomic force microscopy (AFM), the transferred $MoSe_2$ sheet on the $SiO_2$/Si substrate displays a wrinkled morphology (Figure 1f). The line scan at the edge illustrates that the step height is ~0.97 nm (Figure 1g), comparable to previous reports of exfoliated $MoSe_2$ monolayer.[9]

The microstructure of the CVD-grown $MoSe_2$ crystals was probed by selected area electron diffraction (SAED), low-energy electron diffraction (LEED), scanning transmission electron microscopy (STEM), scanning tunneling microscopy (STM), and X-ray photoelectron spectroscopy (XPS). TEM analysis of the edge of a typical triangular $MoSe_2$ crystal transferred onto a copper grid (Figure 2a) reveals that the edge thickness corresponds to a monolayer (Figure 2b). Six

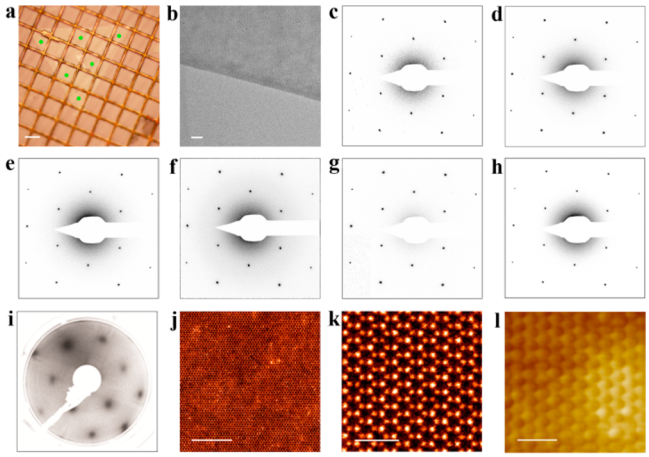


**Figure 2.** Structural characterization of $MoSe_2$ crystals. (a) Optical image of a $MoSe_2$ crystal transferred onto a TEM grid. Scale bar 100 $\mu$m. (b) High-magnification TEM image of the $MoSe_2$ crystal. Scale bar 20 nm. (c–h) Six SAED patterns from the areas labeled in panel a. (i) LEED pattern of a $MoSe_2$ crystal. (j,k) STEM images of $MoSe_2$ crystals with different magnifications. Scale bar 5 nm in panel ) and 1 nm in panel k. The bright spots correspond to Se atoms from the two stacked layers and the dim spots correspond to Mo atoms. (l) STM image of $MoSe_2$ monolayer transferred onto gold substrate, showing the characteristic honeycomb lattice. Scale bar 1 nm.

representative SAED patterns that correspond to different areas labeled in Figure 2a are shown in Figure 2c–h, respectively. The identical orientations of the diffraction patterns across these spatially diverse regions reveal the single-crystal nature.[4b] This result is also confirmed by LEED (Figure 2i) that has a larger analysis spot size (~0.1 mm) than that of SAED (~1 $\mu$m) and provides longer range structural information.[10] The STEM Z-contract images show the atomic resolution of the $MoSe_2$ lattice (Figure 2j,k): a hexagonal pattern with alternating bright and dim atomic sites.[11] No extended structural defects are observed across the film, which confirm the high quality of the $MoSe_2$ monolayer. We also used atomic-resolution STM to verify the atomic structure of the $MoSe_2$ monolayers transferred onto Au films (Figure 2l). STM probes the electron-rich Se atoms, which form a perfect honeycomb lattice with the lattice constant of 3.3 ± 0.1 Å (Figure S6).[12] The absence of atomic defects confirms the high crystalline quality of the $MoSe_2$ samples.

XPS was used to examine the elemental composition and bonding in the $MoSe_2$ samples. The peaks at ~231.5 and 228.3 eV binding energies are attributed to Mo $3d_{3/2}$ and $3d_{5/2}$ core levels (Figure 3a) and the peaks at 55 and 55.9 eV correspond to Se $3d_{5/2}$ and Se $3d_{3/2}$ core levels, respectively (Figure 3b).[11] The signals due to $MoO_3$ were completely absent, suggesting that the surface has a low density of defects and a complete reduction of $Mo^{6+}$ ($MoO_3$) to $Mo^{4+}$ ($MoSe_2$). The ~1:2 Mo/Se ratio obtained from integrated peak areas indicates that the $MoSe_2$ crystals have the desired stoichiometry.

The crystalline quality and optical properties of the $MoSe_2$ crystals were further evaluated using Raman, photoluminescence (PL) and optical absorption measurements. The Raman spectrum shows two characteristic peaks of $MoSe_2$ monolayers: a sharp one at 238.5 $cm^{-1}$ assigned to $A_{1g}$ mode and a broad


DOI: 10.1021/jacs.6b12156
J. Am. Chem. Soc. 2017, 139, 1073–1076

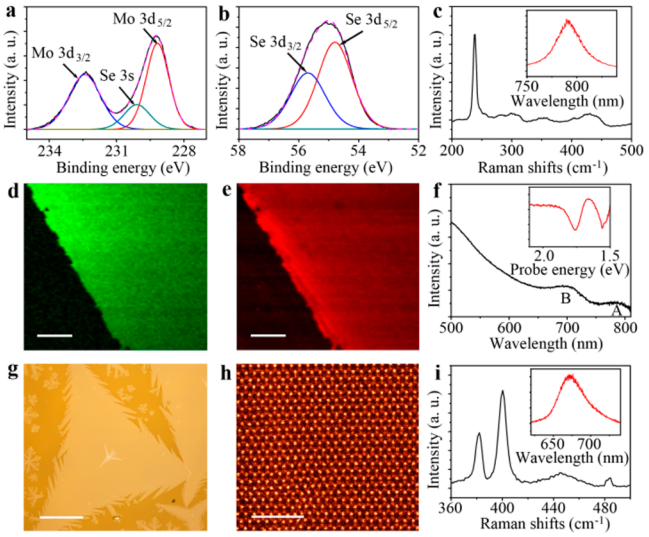


**Figure 3.** Optical and structural characterizations of $MoSe_2$ and $MoS_2$ crystals. (a,b) XPS spectra of $MoSe_2$ transferred onto HOPG showing the Mo 3d core level region (a) and Se 3d core level region (b). (c) Raman spectrum of $MoSe_2$ monolayer. The inset shows the PL spectrum of the crystal. (d,e) Raman (d) and PL (e) spectroscopy maps of the peaks at 238.4 $cm^{-1}$ and 795 nm, respectively. Scale bar 30 $\mu$m. (f) Optical absorption spectrum of $MoSe_2$ crystals. The inset shows the transient absorption spectrum. (g) Optical image of $MoS_2$ monolayer on molten glass. Scale bar 500 $\mu$m. (h) STEM image of $MoS_2$ crystals. Scale bar 2 nm. (i) Raman spectrum of $MoS_2$ monolayer. The inset shows the PL spectrum of the crystal.

one at 284.2 $cm^{-1}$ assigned to $E_{2g}$ mode (Figure 3c).[13] The PL spectrum (Figure 3c, inset) shows a direct band gap PL peak at ~795 nm, corresponding to the direct band gap at K point.[13] The spatial dependences of Raman and PL signals extracted from the integrated intensities of the characteristic Raman (238.4 $cm^{-1}$) and PL (795 nm) peaks were plotted in Figure 3d and 3e. The uniform color intensity is a reliable indicator of the uniform thickness.

Figure 3f displays the optical absorption spectrum of the $MoSe_2$ monolayers. Two excitonic absorption peaks A and B, arising from direct gap transitions at the K point, are identified at ~795 and 700 nm, respectively.[14] A millimeter-sized $MoSe_2$ monolayer allows us to measure directly the transient absorption spectra and relaxation lifetimes using a conventional pump−probe setup. The transient absorption spectrum after 500 nm pumping yields typical $MoSe_2$ spectral features in the visible range (500−800 nm): two photobleaching peaks (PB, $\Delta T/T > 0$ or $\Delta A < 0$) at around 700 nm (1.77 eV) and 795 nm (1.56 eV) and two photoinduced absorption (PA, $\Delta T/T < 0$ or $\Delta A > 0$) band over the 525−650 nm and 725−775 nm regions. The PA bands are due to carrier-induced excited-state peak broadening.[15] The PB peaks at 1.56 and 1.77 eV correspond to the A and B excitons (Figure 3f).[14] The dynamics of both excitons show ultrafast rise times of around 200 fs, and then undergo a multiexponential decay (Figure S7). The ultrafast rise and decay dynamics of the large-sized $MoSe_2$ monolayer can be exploited for photonics applications.

To assess the generality of the "molten glass substrate" approach for growing other TMDs, we have also applied it to synthesize $MoS_2$ crystals. The parameters and procedure for $MoS_2$ growth are similar to that of $MoSe_2$ except that S (instead of Se) is used as precursor. The introduction of $H_2$ flow is not required due to the stronger chemical reactivity of S. Figure 3g shows the OM image of large-size $MoS_2$ monolayers grown on molten glass. Different from that of $MoSe_2$, the triangular $MoS_2$ crystal displays three jagged edges due to S-zigzag edge orientations.[7] The size of the as-grown $MoS_2$ crystals can reach 2.6 mm (Figure S8), which is larger than that of all the previously reported TMDs.[4,7,11] We also characterized the $MoS_2$ lattice using STEM (Figure 3h). Different from that of $MoSe_2$ crystals, the bright spots, here, correspond to Mo atoms and the dim spots correspond to S atoms from the two layers sandwiching the inner Mo atoms. Figure 3i shows the Raman spectrum of the $MoS_2$ crystals. The $A_{1g}$ and $E_{2g}$ modes of $MoS_2$ monolayer are located at ~400.1 and ~382.2 $cm^{-1}$, respectively.[16] The PL spectrum (Figure 3i, inset) shows the characteristic emission peaks of $MoS_2$ monolayers at ~673 nm, corresponding to the direct excitonic transition of $MoS_2$ monolayer.[16]

Interestingly, the size of our TMD crystals grown on molten glass is more than 3 orders of magnitude larger than that of graphene nanodisks,[6] suggesting that a different growth mechanism is in place. All the crystals grown have a triangular morphology, and adjacent crystals formed twin-crystal structure (Figure S4). The growth kinetics is similar to that occurring on solid substrates, which suggests a similar surface deposition process. However, a high density of $MoSe_2$ crystallites were grown on "solid-state" glass and $SiO_2$/Si substrates (Figure S9), with sizes which are 1 order smaller compared to the crystals grown on molten glass. Because the nucleation of crystallites occurs preferentially at impurities or defect sites, it follows that creating a homogeneous surface will reduce the density of nucleation sites, thus promoting the growth of large-size crystals. We found that the surface of the solid-state glass is usually rough; however, glass melts above 750 °C, allowing a quasi-atomic smooth and homogeneous liquid surface to be regenerated (Figure S10). Uniquely, the "molten glass substrate" approach suppresses nucleation event without the need to reduce feedstock supply,[4b] thus it does not compromise the high rate growth of large-size high-quality TMD crystals from the nuclei. Molten glass has a nonperiodic ionic structure which is time-dependent, the thermal ionic motion causes the fluctuation of the interatomic distance, which weakens the interaction between adatoms and growth substrates, and thus lowers the migration barrier energy ($U$) of adatoms. The migration coefficient $D$ is related to $U$ by

$$D \approx D_{\infty}\exp(-U/k_{B}T)$$

where $k_B$ is the Boltzmann constant and $T$ is the temperature.[17] The migration coefficient on molten glass is far lower than that on solid substrates. Therefore, a high growth rate, together with a low nucleation density, contributes to the formation of millimeter-size $MoSe_2$ and $MoS_2$ crystals on molten glass. Further studies will be needed to elucidate the detailed growth mechanism.

To investigate the electrical properties of the as-grown $MoSe_2$ crystals, back-gate FETs were fabricated on $SiO_2$/Si substrates (Figure 4a). The $I-V$ characteristics of a typical device with a channel length ($L$) of ~10 $\mu$m and a channel width ($W$) of ~2 $\mu$m, measured in a vacuum, is shown in Figure 4b. The linear and symmetric curves suggest that ohmic-like contacts are formed at the source and drain electrodes. Figure 4c shows the transfer curves driven at different $V_{DS}$. The $I_{DS}$ value increases monotonically with increasing $V_G$, which is indicative of $n$-type behavior. The maximum on/off current ratio is ~$10^7$, and the threshold voltage is around −20 V


DOI: 10.1021/jacs.6b12156
J. Am. Chem. Soc. 2017, 139, 1073−1076

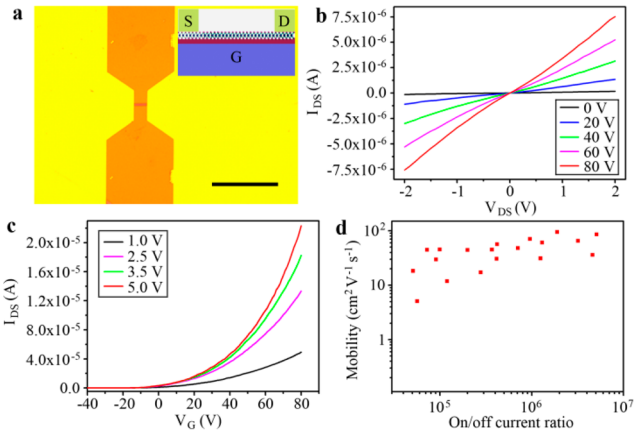


**Figure 4.** $MoSe_2$ FET devices. (a) Optical image of a $MoSe_2$ FET. Scale bar 50 $\mu$m. The inset shows a schematic diagram of this device. (b) $I_{DS}$–$V_{DS}$ characteristics for the device. (c) Transfer characteristics ($I_{DS}$ vs $V_G$) of the device at different $V_{DS}$. (d) The distributions of on/off current ratios and mobilities of 19 $MoSe_2$ FETs.

(Figure S11). The carrier mobility can be calculated from the linear regime of the transfer characteristics. Analyzing the transport characteristics of 19 $MoSe_2$ FETs, the mobility and the on/off current ratios were determined to be in the range of 5–95 $cm^2 V^{-1} s^{-1}$ and $10^4$–$10^7$, respectively (Figure 4d), which are comparable to the values of mechanically cleaved $MoSe_2$,[11,18] and confirm the high crystalline quality of our $MoSe_2$ crystals. The carrier mobility can be further improved by optimizing device structure and interface engineering.[3b]

In summary, by using molten glass as growth substrates, we have achieved the fast growth of millimeter-size monolayer $MoSe_2$ and $MoS_2$ crystals. The advantage of molten glass is the generation of a low-defect, highly homogeneous template with low nucleation density. The largest monolayer $MoSe_2$ and $MoS_2$ crystals synthesized have lateral dimensions of ~2.5 mm, which is larger than that of all the previously reported TMDs.[4,7,11] Atomic-scale imaging and optical/electrical transport studies have confirmed the high crystalline quality of these samples. Our results provide a new direction to the synthesis of large-size $MoSe_2$ and $MoS_2$ crystals on low-cost molten glass substrates, and form the basis of a versatile approach for the synthesis of 2D TMDs. Our work further points to the possibilities of using other "liquid-state" substrates for the growth of 2D materials.

## ■ ASSOCIATED CONTENT

### Supporting Information

The Supporting Information is available free of charge on the ACS Publications website at DOI: 10.1021/jacs.6b12156.

Experimental procedures and additional figures (PDF)

## ■ AUTHOR INFORMATION


### Corresponding Author

*chmlohkp@nus.edu.sg

### ORCID

Jianyi Chen: 0000-0002-3757-7634

Kian Ping Loh: 0000-0002-1491-743X


### Notes

The authors declare no competing financial interest.

## ■ ACKNOWLEDGMENTS

The authors acknowledge support by National Research Foundation, Singapore, Midsized Centre grant (CA2DM) under the Prime Minister's Office. The electron microscopy work was supported in part by the U.S. Department of Energy, Office of Science, Basic Energy Science, Materials Sciences and Engineering Division (W.Z.), and through a user project at ORNL's Center for Nanophase Materials Sciences (CNMS), which is a DOE Office of Science User Facility.

## ■ REFERENCES


(1) Wang, Q. H.; Kalantar-Zadeh, K.; Kis, A.; Coleman, J. N.; Strano, M. S. *Nat. Nanotechnol.* **2012**, *7*, 699.

(2) Zhu, Z. Y.; Cheng, Y. C.; Schwingenschlögl, U. *Phys. Rev. B: Condens. Matter Mater. Phys.* **2011**, *84*, 153402.

(3) (a) Yin, Z.; Li, H.; Li, H.; Jiang, L.; Shi, Y.; Sun, Y.; Lu, G.; Zhang, Q.; Chen, X.; Zhang, H. *ACS Nano* **2012**, *6*, 74. (b) Radisavljevic, B.; Radenovic, A.; Brivio, J.; Giacometti, V.; Kis, A. *Nat. Nanotechnol.* **2011**, *6*, 147. (d) Zeng, H.; Dai, J.; Yao, W.; Xiao, D.; Cui, X. *Nat. Nanotechnol.* **2012**, *7*, 490.

(4) (a) Chen, W.; Zhao, J.; Zhang, J.; Gu, L.; Yang, Z.; Li, X.; Yu, H.; Zhu, X.; Yang, R.; Shi, D.; Lin, X.; Guo, J.; Bai, X.; Zhang, G. *J. Am. Chem. Soc.* **2015**, *137*, 15632. (b) Gao, L.; Ren, W.; Xu, H.; Jin, L.; Wang, Z.; Ma, T.; Ma, L.-P.; Zhang, Z.; Fu, Q.; Peng, L.-M.; Bao, X.; Cheng, H.-M. *Nat. Commun.* **2012**, *3*, 699.

(5) Geng, D.; Wu, B.; Guo, Y.; Huang, L.; Xue, Y.; Chen, J.; Yu, G.; Jiang, L.; Hu, W.; Liu, Y. *Proc. Natl. Acad. Sci. U. S. A.* **2012**, *109*, 7992.

(6) Chen, Y.; Sun, J.; Gao, J.; Du, F.; Han, Q.; Nie, Y.; Chen, Z.; Bachmatiuk, A.; Priydarshi, M. K.; Ma, D.; Song, X.; Wu, X.; Xiong, C.; Rümmeli, M. H.; Ding, F.; Zhang, Y.; Liu, Z. *Adv. Mater.* **2015**, *27*, 7839.

(7) van der Zande, A. M.; Huang, P. Y.; Chenet, D. A.; Berkelbach, T. C.; You, Y.; Lee, G.-H.; Heinz, T. F.; Reichman, D. R.; Muller, D. A.; Hone, J. C. *Nat. Mater.* **2013**, *12*, 554.

(8) Zhou, Y.; Deng, B.; Zhou, Y.; Ren, X.; Yin, J.; Jin, C.; Liu, Z.; Peng, H. *Nano Lett.* **2016**, *16*, 2103.

(9) Tonndorf, P.; Schmidt, R.; Böttger, P.; Zhang, X.; Börner, J.; Liebig, A.; Albrecht, M.; Kloc, C.; Gordan, O.; Zahn, D. R.; Michaelis de Vasconcellos, S.; Bratschitsch, R. *Opt. Express* **2013**, *21*, 4908.

(10) Mahatha, S. K.; Patel, K. D.; Menon, K. S. *J. Phys.: Condens. Matter* **2012**, *24*, 475504.

(11) Wang, X.; Gong, Y.; Shi, G.; Chow, W. L.; Keyshar, K.; Ye, G.; Vajtai, R.; Lou, J.; Liu, Z.; Ringe, E.; Tay, B. K.; Ajayan, P. M. *ACS Nano* **2014**, *8*, 5125. (b) Gong, Y.; Ye, G.; Lei, S.; Shi, G.; He, Y.; Lin, J.; Zhang, X.; Vajtai, R.; Pantelides, S. T.; Zhou, W.; Li, B.; Ajayan, P. M. *Adv. Funct. Mater.* **2016**, *26*, 2009.

(12) Huang, Y. L.; Chen, Y.; Zhang, W.; Quek, S. Y.; Chen, C.-H.; Li, L.-J.; Hsu, W.-T.; Chang, W.-H.; Zheng, Y. J.; Chen, W.; Wee, A. T. S. *Nat. Commun.* **2015**, *6*, 6298.

(13) (a) Xia, J.; Huang, X.; Liu, L.-Z.; Wang, M.; Wang, L.; Huang, B.; Zhu, D.-D.; Li, J.-J.; Gu, C.-Z.; Meng, X.-M. *Nanoscale* **2014**, *6*, 8949. (b) Shaw, J. C.; Zhou, H.; Chen, Y.; Weiss, N. O.; Liu, Y.; Huang, Y.; Duan, X. *Nano Res.* **2014**, *7*, 511.

(14) Su, S.-H.; Hsu, W.-T.; Hsu, C.-L.; Chen, C.-H.; Chiu, M.-H.; Lin, Y.-C.; Chang, W.-H.; Suenaga, K.; He, J.-H.; Li, L.-J. *Front. Energy Res.* **2014**, *2*, 27.

(15) Shi, H.; Yan, R.; Bertolazzi, S.; Brivio, J.; Gao, B.; Kis, A.; Jena, D.; Xing, H. G.; Huang, L. *ACS Nano* **2013**, *7*, 1072.

(16) Lee, Y.-H.; Zhang, X.-Q.; Zhang, W.; Chang, M.-T.; Lin, C.-T.; Chang, K.-D.; Yu, Y.-C.; Wang, J. T. -W.; Chang, C.-S.; Li, L.-J.; Lin, T.-W. *Adv. Mater.* **2012**, *24*, 2320.

(17) Einax, M.; Dieterich, W.; Maass, P. *Rev. Mod. Phys.* **2013**, *85*, 921.

(18) Larentis, S.; Fallahazad, B.; Tutuc, E. *Appl. Phys. Lett.* **2012**, *101*, 223104.




DOI: 10.1021/jacs.6b12156
J. Am. Chem. Soc. 2017, 139, 1073–1076